Pharm Res (2014) 31:3348–3360
DOI 10.1007/s11095-014-1424-1

RESEARCH PAPER

Rapidly Dissolvable Microneedle Patches for Transdermal Delivery of Exenatide

Zhuangzhi Zhu • Huafei Luo • Wangding Lu • Hansen Luan • Yubo Wu • Jing Luo • Youjie Wang • Jiaxin Pi • Chee Yen Lim • Hao Wang

Received: 17 March 2014 / Accepted: 12 May 2014 / Published online: 28 May 2014

ABSTRACT

Purpose To assess the feasibility of transdermal delivery of exenatide (EXT) using low-molecular-weight sodium hyaluronate (HA) dissolving microneedles (MNs) patches for type 2 diabetes mellitus therapy.

Methods Micromold casting method was used to fabricate EXT-loaded dissolving MNs. The characteristics of prepared MNs including mechanical strength, *in vitro/in vivo* insertion capacity, dissolution profile and storage stability were then investigated. Finally, the *in vivo* pharmacokinetics and hypoglycemic effects were compared with traditional subcutaneous (SC) injection.

Results EXT-loaded dissolving MNs made of HA possessed sufficient mechanical strength and the strength could be weakened as the water content increases. The EXT preserved its pharmacological activity during fabrication and one-month storage. With the aid of spring-operated applicator, dissolving MNs could be readily penetrated into the skin *in vitro/in vivo*, and then rapidly dissolved to release encapsulated drug within 2 min. Additionally, transepidermal water loss (TEWL) determinations showed that skin's barrier properties disrupted by MNs recovered within 10–12 h. Transdermal pharmacokinetics and antidiabetic effects studies demonstrated that fabricated EXT MNs induced comparable efficacy to SC injection.

Conclusions Our rapidly dissolving MNs patch appears to an excellent, painless alternative to conventional SC injection of EXT, and this minimally invasive device might also be suitable for other biotherapeutics.

KEY WORDS dissolving microneedles · exenatide · pharmacokinetics/pharmacodynamics · transdermal delivery · type 2 diabetes mellitus

ABBREVIATIONS

EXT	Exenatide
FAM-EXT	Carboxyfluorescein-labeled exenatide
GLP-1	Glucagon-like peptide-1
HA	Sodium hyaluronate
MNs	Microneedles
OGTT	Oral glucose tolerance test
PDMS	Polydimethylsiloxane
RBA	Relative bioavailability
SC	Subcutaneous
TEWL	Transepidermal water loss
UPLC-MS/MS	Ultra-performance liquid chromatography tandem mass spectrometry

Z. Zhu • H. Luo • W. Lu • H. Luan • Y. Wu • J. Luo • J. Pi • H. Wang (✉)
National Pharmaceutical Engineering Research Center, China
State Institute of Pharmaceutical Industry, 1111 Ha
Lei Road, Shanghai 201203, China
e-mail: wanghao99@hotmail.com

Z. Zhu
e-mail: zhuzz918@126.com

Y. Wang
Engineering Research Center of Modern Preparation Technology of TCM, Ministry of Education, Shanghai University of Traditional Chinese Medicine, Shanghai 201203, China

C. Y. Lim
Micropoint Technologies Pte. Ltd., #02-10 CleanTech One, Singapore 637141, Singapore

INTRODUCTION

Type 2 diabetes mellitus is a chronic metabolic disorder characterized by relative deficiency of insulin secretion and decreased insulin sensitivity (1). This type of diabetes, which also refers to as non-insulin-dependent diabetes, accounts for approximately 90–95% of all diabetic patients (2). Therefore, the development of hypoglycemic drugs and relevant formulations has become increasingly important. Exenatide (EXT), a first-in-class incretin mimetic, is a synthetic product of exendin-4 originally isolated from the salivary secretions of the lizard

Heloderma suspectum. It is a 39-amino acid peptide, which shares 53% sequence homology with the mammalian glucagon-like peptide-1 (GLP-1) (3,4). As a highly potent GLP-1 receptor agonist, EXT has been approved as a therapy for type 2 diabetes mellitus, marketed as twice-daily Byetta® and once-weekly Bydureon® (both Amylin Pharmaceuticals, San Diego, CA, USA). Bydureon® is a long-acting microsphere formulation of EXT and reduces administration frequency to some extent (5). However, both products have to be administrated by subcutaneous (SC) injection, which could cause pain, needle phobia and infections at the injection sites, resulting in poor patient compliance (6).

To address this issue, minimally invasive delivery routes of EXT without a hypodermic needle, including oral, sublingual, intranasal and pulmonary routes, have been investigated as alternatives to parenteral route (6–10). However, compared to traditional SC injection, the absorption of EXT from these routes into the systemic circulation is still poor owing to presystemic enzymatic degradation and penetration barriers present in epithelial mucosa (11). Transdermal delivery is poised to provide an attractive alternative because of its easy accessibility, non-invasion, painless administration, potential for self-administration and avoidance of first-pass effect. Most drugs, however, especially for macromolecules, do not penetrate skin at therapeutically relevant doses due to the biological barrier imposed primarily by skin's outermost *stratum corneum* layer. To overcome this barrier, a variety of strategies have been developed to increase percutaneous absorption of macromolecular therapeutics, such as chemical enhancers, liquid/powder jet injections, iontophoresis, electroporation, microdermabrasion, ultrasound, thermal ablation and microneedles (MNs) (12–14).

MNs are arrays of micron-scale needles that permeabilize the *stratum corneum* by creating reversible microchannels in the skin, thereby enabling the penetration of skin-impermeant biotherapeutics. These minimally invasive devices are long enough to pierce through the permeability barrier, but short and thin enough to avoid causing pain (15). MNs with diverse geometries have been made of various materials including silicon, metals, glass and polymers. Four different types of MNs strategies have been developed: 1) solid MNs for skin pretreatment to enhance permeability; 2) coated MNs with drug coating that dissolves off in the skin; 3) dissolving MNs that incorporate drug and dissolve in the skin; 4) hollow MNs for drug solution injection (16,17). Each type of MNs has specific advantages and limitations.

In the last few years, dissolving MNs have received extensive attention because of the following potential advantages over other types of MNs: 1) in contrast to coated MNs, dissolving MNs encapsulate sensitive biomolecules within the needle shafts, which may exhibit a higher loading capacity; 2) dissolving MNs made out of water-soluble biocompatible polymers dissolve upon insertion into the skin, thereby leaving no sharp biohazardous waste after use; 3) using relatively inexpensive polymers and micromold casting method, dissolving MNs can be readily produced in an economical manner suitable for scale up to mass production (16–19). However, water-soluble polymers generally have weaker mechanical strength compared to non-dissolving materials like silicon or metal, and drug encapsulation may further weaken their biomechanical strength (18,19). Thus, proper geometry design and materials selection are particularly important for dissolvable MNs fabrication. To date, dissolving MNs have been fabricated from various materials, such as sugars (20,21), carboxymethylcellulose (18,22), polyvinylpyrrolidone (23), poly (methyl vinyl ether-maleic acid) (19), chondroitin sulfate (24) and sodium hyaluronate (HA) (13,25–28).

In this study, we selected HA as water-soluble matrix material of the EXT dissolving MNs patches. HA is a biocompatible polysaccharide that can be found abundantly in all tissues and body fluids, especially in the skin (29). This natural biopolymer is widely used as a cosmetic ingredient in skin care products and injectable filler for soft tissue augmentation (28,30). Moreover, HA was found to produce MNs with sufficient mechanical strength and high safety in human (13,27,28). Therefore, its high hydrophilicity and biocompatibility make HA an excellent candidate for dissolving MNs material. In the present study, we first developed novel EXT-loaded dissolving MNs made of HA. The characteristics of prepared MNs including mechanical property, insertion capacity, dissolution profile and storage stability were then investigated. Finally, the *in vivo* pharmacokinetics and hypoglycemic effects were evaluated. This is the first study to translate the use of dissolving MNs patches for transdermal delivery of EXT, which might significantly enhance patient compliance.

MATERIALS AND METHODS

Materials and Animals

EXT was kindly provided by Shanghai Institute of Pharmaceutical Industry (Shanghai, China). HA with molecular weight less than 10 kDa (miniHA^{TM}) was obtained from Bloomage Freda Biopharm Co., Ltd. (Jinan, China). Polydimethylsiloxane (PDMS, Sylgard® 184) and carboxyfluorescein-labeled EXT (FAM-EXT, Abs/Em=494/519 nm) were purchased from Dow Corning Corp., (Midland, USA) and AnaSpec, Inc., (San Jose, CA, USA), respectively. Exenatide enzyme immunoassay (EIA) kits were provided by Phoenix Pharmaceuticals, Inc. (EK-070-94, CA, USA). Other chemicals and reagents used were of analytical reagent grade and supplied by Sinopharm Chemical Reagent Co., Ltd. (Shanghai, China).

Fresh neonatal porcine skin was obtained from a local slaughterhouse. Male Sprague–Dawley (SD) rats with body weight of 200–250 g were supplied by the Shanghai Super-B&K Laboratory Animal Corporation Ltd. (Shanghai, China), and

male C57BL/6 J *db/db* mice (5–8 weeks old) were obtained from the Model Animal Research Center of Nanjing University (Nanjing, China). The animals were housed under controlled conditions of 12:12 h light–dark cycle and 22 ± 2°C, with food and water *ad libitum*. All studies concerning experimental animals were conducted in accordance with Ethical Guidelines for Investigations in Laboratory Animals and were approved by National Pharmaceutical Engineering and Research Center.

Preparation of Drug-loaded Dissolving MNs

The dissolving MNs were prepared via micromold-based method as previously reported (18,19,24). Briefly, a stainless steel master structure consisted of 225 pyramidal needles (with approximately 600 μm height, 200 μm width at base, 500 μm interspacing, and 15 × 15 array) was created using an electrical discharge machining process (Micropoint Technologies Pte. Ltd., Singapore). After placing the master structure in the centre of a metal mould, degassed PDMS (mixed in a 10:1 *w/w* ratio of prepolymer to curing agent) was poured into the mould, and cured for 1 h at 90°C. The precisely inverse-replicated micromolds were then obtained by peeling off the master structure carefully.

To serve as the MNs casting material, 0.5 g of HA was dissolved in 1.0 mL of distilled water and mixed with EXT or FAM-EXT. Thirty μL of the prepared drug-load solution was added to the surface of the micromold in a 50-mL Corning tube and centrifuged (TDZ5-WS, Shanghai Lu Xiangyi Centrifuge Instrument Co., Ltd., China) at 4,390 × *g* for 1 min to push the casting solution into the cavities of the mold. Excess solution remaining on the surface was pipetted and saved for recycling use. The micromold was then centrifuged for 5 min to facilitate compaction and drying. A blank solution consisting of 1.0 g of HA and 1.0 mL of distilled water was dispensed onto the mold and centrifuged to form the backing layer. After dried in the desiccator containing silica gel at room temperature, the EXT-loaded MNs patches were detached from the micromold (Fig. 1). Placebo dissolving MNs were also prepared by the same method, except that no drug was added. Thereafter, the obtained MNs patches were examined by a digital microscope (VHX-1000, Keyence Corp., Osaka, Japan).

Quantification of EXT in the MNs Patches

To determine the contents of EXT loaded in the MNs patches, drug was extracted from each patch with 10.0 mL of deionized water followed by vortex mixing to release the encapsulated drug completely. After centrifuged for 10 min, the supernatant was separated and analyzed by ultra-performance liquid chromatography tandem mass spectrometry (UPLC-MS/MS) described below.

Mechanical Properties of HA Dissolving MNs

The TA.XT *plus* texture analyzer (Stable Micro Systems, Surrey, UK) was used to study the mechanical properties of prepared HA MNs patches. Each tested MNs patch (placebo or drug-loaded) was placed on the flat rigid aluminium plate with the needle tips upward. An axial force oriented

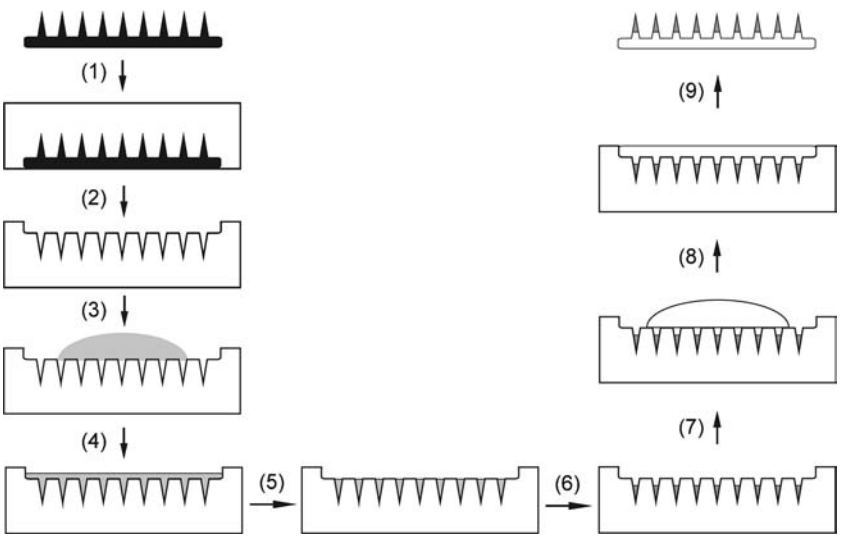

Fig. 1 Schematic illustration of the fabrication process of HA dissolving MNs patches fabrication process. (1) PDMS was poured onto the stainless steel master structure; (2) PDMS micromold was cured and peeled off the master structure; (3) drug-loaded solution was added to the surface of the micromold; (4) micromold was centrifuged to push the casting solution into the cavities of the mold; (5) excess solution remaining on the surface was removed; (6) the mold was centrifuged to facilitate compaction and drying; (7) blank solution was dispensed onto the mold; (8) blank solution was centrifuged to form the backing layer; (9) the drug-loaded MNs patch was dried and detached from the mold after dried.

perpendicularly to the plate (i.e. parallel to the MNs vertical axis) was then applied using a 5-mm-diameter flat-head stainless steel cylindrical probe to press against the tips of the MNs array at a constant speed of 1.1 mm/sec, and the trigger force was set at 0.049 N (13,18). The texture analyzer recorded the force required to move the metal cylinder as a function of distance until a preset displacement of 400 μm was reached.

To evaluate the effect of residual water content in dissolving MNs on needle strength, various moisture contents of MNs patches were generated by incubating the MNs with saturated salt solutions in desiccators at room temperature (13,25). The relative humidity (RH) in the desiccators was maintained at 23, 33, 43 and 75% through the use of saturated salt solutions (CH_3COOK, $MgCl_2$, K_2CO_3 and NaCl) (13,31). After at least 3 days, water contents in the MNs were first analyzed using drying loss method on the electronic moisture balance (MOC-120H, Shimadzu Corporation, Kyoto, Japan). The mechanical strengths of different water contents MNs were then determined as described above.

In Vitro and *In Vivo* Imaging of MNs Insertions

To assess the *in vitro* skin insertion capability of the prepared MNs, neonatal porcine skin was separated from stillborn piglets and immediately excised, trimmed to an appropriate thickness. A 15×15 array of MNs patch co-loaded with EXT and methylene blue (0.5%, *w/v*) was attached to a home-made spring-operated applicator and then inserted into the porcine cadaver skin for approximately 2 min to dissolve the encapsulated drug and dye. After the MNs were removed, the punctured skin was imaged under the stereomicroscope to calculate the insertion ratio by dividing the number of blue dots on the skin after insertion by the number of needles in a MNs array (32).

To determine the depth of MNs insertion, FAM-EXT-loaded MNs were pierced into the porcine skin as described above. The treated areas were isolated from the skin with a surgical scalpel. The excised skin samples were covered with an O.C.T. compound (Tissue-Tek®, Sakura Finetek USA, Inc., Torrance, CA) in an embedding mold and snap-frozen in liquid nitrogen. The frozen samples were sectioned into 10-μm-thick serial slices on a Leica CM1950 cryostat microtome (Leica Microsystems, Nussloch, Germany) and these sections were mounted onto positively charged microscope slides (Citotest Labware Manufacturing Co., Ltd., China). The skin sections were then examined under an Olympus IX-81 inverted fluorescence microscope (Olympus Corp., Tokyo, Japan).

In vivo MNs insertions were conducted on SD rats. The hair on the back region was carefully removed with electric shaver and depilatory cream (Veet®, Reckitt Benckiser Household Products Co., Ltd., Beijing, China) under anesthesia the day before the experiment. FAM-EXT-loaded MNs were applied to the exposed skin and left for 2 min to dissolve the MNs. Rats were euthanized immediately and the skin was harvested using a surgical scissors. Full thickness skin was carefully excised by removing excess subcutaneous fat and connective tissue. The obtained skin samples were placed on a glass slide and examined using a Zeiss LSM 710 confocal laser scanning microscope system (Carl Zeiss MicroImaging, Germany) under excitation at 494 nm to visualize the vertical distribution of the drug in the skin. Images were captured in the *xy*-plane (i.e., parallel to the plane of the skin surface). The initially scanned skin surface ($z=0$ μm) was defined as the imaging plane of the outermost *stratum corneum* layer. Scanning was conducted once at an interval of 10 μm from the skin surface through the *z*-axis perpendicular to the *xy*-plane (32).

In Vitro Dissolution of Drug from the EXT-loaded MNs

EXT-loaded MNs patches were inserted into neonatal porcine skins using the home-made applicator and held *in situ* for varying time intervals (1, 3, 5, 10, 30, 60, 90, 120, 150 and 180 sec). After removal of the MNs, the punctured area were tape-stripped twice with Scotch® tape (3 M Company, MN, USA) to remove the residual drug left on the skin surface. Both the inserted MNs and stripped tapes were soaked in 10.0 mL of deionized water for 10 min at room temperature to recover the drug. The extracted solutions were then assayed by an established UPLC-MS/MS method. Using a mass balance, the amount of drug delivered into the skin was calculated by subtracting the amount of EXT remaining in the MNs after insertion and on the skin surface from the amount initially loaded in the non-inserted MNs patches (13,32).

UPLC-MS/MS Assay Method for EXT

The resultant EXT samples were determined using a UPLC-MS/MS system (33), which consisted of a Waters Acquity™ UPLC and a Xevo™ TQ MS triple-quadrupole mass spectrometer (Waters Corp., MA, USA). Chromatographic separation was achieved under gradient conditions employing 0.2% formic acid in deionized water (A) and 0.2% formic acid in acetonitrile (B) at a flow rate of 0.2 mL/min using an Acquity BEH300 C18 Peptide Separation Technology column (2.1 mm×50 mm, 1.7 μm, Waters Corp., MA, USA) at 50°C. Initial conditions were 80% (A) then ramped to 75% (B) over 1.5 min, held for 1.0 min then back to initial conditions. The injection volume was 3.0 μL and the total cycle time was 3.0 min. The MS/MS acquisitions were performed in positive ion electrospray ionization (ESI) mode with multiple reaction monitoring (MRM). A tuning software, IntelliStart™, was used to automatically optimize source voltages and fragment generation and selection for the analyte. For EXT detection, the characteristic precursor $[M+4H]^{4+}$ to product ion transition of m/z 1047.6→396.4 was optimized for the following parameters: capillary voltage, cone voltage and collision energy with 3.00 kV, 36 V and 34 eV, respectively; desolvation

gas flow with 1,000 L/h; source and desolvation temperature with 150 and 500°C, respectively; dwell time with 0.100 sec.

Transepidermal Water Loss (TEWL) Determinations after the Dissolving MNs Insertion

The hair on the dorsal region was removed the day before the experiment. After anesthetized and acclimatized to the ambient conditions (i.e., 20±2°C, 50±5% RH) for 30 min, the exposed skin was treated with EXT dissolving MNs as previously described. The Tewameter® TM 300 (Courage + Khazaka electronic GmbH, Cologne, Germany) was used to determine TEWL at the treated sites pre- (0.25 h prior to MNs treatment) and post-application of MNs. TEWL determinations were performed at different time points (0, 0.25, 0.5, 1, 2, 3, 4, 6, 8, 10 and 12 h after removal of MNs) by placing the probe head horizontally on the treated skin at a constant pressure. Meanwhile, TEWL measurements were also taken for the control group (n=6 for each group) which received the same protocol except MNs treatment.

Storage Stability of EXT Encapsulated in Dissolving MNs Patches

To assess the storage stability of EXT-loaded MNs, MNs patches were first heat sealed in aluminum plastic-laminated sachets containing silica gel, and then stored under various temperatures (−20, 4, 25 and 40°C) for 1 month. Thereafter, MNs were dissolved in deionized water, and residual EXT contents were determined as described above.

In Vivo Pharmacokinetic Studies in SD Rats

After 1 week of acclimation, each rat was anesthetized by an intraperitoneal injection of sodium pentobarbital (50 mg/kg), and the back hair was removed as described previously. Prior to the experiment, rats were fasted overnight, but received water *ad libitum*. Animals were randomly divided into three groups (n=4 for each): 1) the SC injection group; 2) the EXT-loaded MNs (5 μg per patch) group; 3) the transdermal solution group. For the SC injection group, Byetta® prefilled pen, an EXT injectable prescription medicine (5 μg/20 μL per dose), was subcutaneously injected into dorsal skin using 31-gauge disposable pen needles. MNs patches were administered to the rat skin using the applicator. For the transdermal group, 20 μL of EXT solution (5 μg/20 μL, the same concentration as Byetta®) was spread evenly on the exposed skin of each mouse, and the applied area was then covered with air-permeable tape to prevent animal licking. The rats were given free access to water during the experiment. Blood samples (approximately 0.2 mL) were collected by retro-orbital bleeding into heparin anticoagulated polyethylene tubes at predetermined time points (0, 0.25, 0.5, 0.75, 1, 1.5, 2, 3, 4 and 5 h after administration). After centrifugation at 12,750× *g* for 3 min, the supernatant plasma was obtained and stored at −80°C until analysis. Plasma concentrations of EXT were quantified using commercial EXT EIA kits, followed by the manufacturer's instructions (7,8).

The maximum drug concentration, C_{max}, and the time to reach maximum plasma EXT concentration, T_{max}, were determined from curves obtained by plotting the drug concentration (ng/mL) *versus* time. The area under the plasma concentration-time curve, AUC, was computed by the trapezoid method and used to calculate bioavailability. The relative bioavailability (RBA) of the EXT-loaded MNs was calculated using the following formula:

$$RBA = (AUC_{MN} \times Dose_{SC})/(AUC_{SC} \times Dose_{MN}) \times 100\%$$

where AUC_{MN} and AUC_{SC} signify the areas under the curves after applying the drug-loaded MNs patches and subcutaneous injection of EXT solution, respectively (25).

Hypoglycemic Effects of EXT-loaded MNs Patches

Diabetic *db/db* mice were first used to evaluate the hypoglycemic effects of EXT-loaded MNs patches under non-fasting conditions with free access of water and food (9,34). After removed the dorsal hair, three groups (n=6 for each) of mice were treated respectively with placebo MNs (control), drug-loaded MNs patches or SC injections (5 μg EXT per mouse). Blood glucose levels were then monitored using a glucometer (Accu-Chek Performa Nano, Roche Diagnostics, Germany) by tail vein blood sampling at 0, 0.5, 1, 2, 3, 4, 5, 6, 8, 10 and 12 h after administration.

The glucoregulatory effects of EXT MNs patches were further examined using oral glucose tolerance test (OGTT) in type 2 *db/db* mice after administration, as previously reported (7,34). Briefly, overnight-fasted mice were randomly divided into four treatment groups (n=5 for each): the placebo MNs group (blank control), the EXT MNs group, the SC injection group and the transdermal solution group (5 μg EXT per mouse). Mice in these four groups were treated with different dosage regimens described above at −0.5 h. At 0 h, intragastric administration of a glucose solution (1.0 g/10 mL/kg) was performed in each mouse, and blood glucose levels were then determined at set intervals (−30, 0, 15, 30, 45, 60, 90, 120 and 180 min post-glucose administration). The mice were given free access to water, but remained fasted throughout the entire experiment. Long-term antidiabetic efficacy of EXT dissolving MNs was then evaluated in a separate set of experiments. Three groups (n=5 for each) of animals were treated respectively with blank MNs, SC injections or EXT-loaded MNs twice everyday (10:00 am and 5:00 pm, 5 μg EXT per mouse once) for 2 weeks (Day 1-

Day 14). MNs patches were applied alternately to the bilateral dorsal skin of mice. To carry out OGTT, the mice were fasted from 9:00 am for 4 h, followed by an oral administration of glucose solution described above. Blood glucose levels were monitored at 0 (before glucose administration), 30 and 60 min after the glucose administration (38). Meanwhile, the MNs application areas were observed throughout the entire study period to assess the local skin tolerability.

Statistical Analysis

Data are presented as mean value ± standard deviation. Statistical data were analyzed by Student's *t*-test or one-way analysis of variance using SPSS version 16.0. Statistical differences were assumed to be significant when $p<0.05$.

RESULTS

Characterization of Fabricated HA MNs

Micromolding method was used to fabricate the EXT-loaded dissolving MNs patches (Fig. 1). PDMS micromolds were first inverse-replicated from the stainless steel master structure (Fig. 2a). These micromolds were then used to replicate dissolving MNs by solvent casting with aqueous solution of HA, resulting in rigid MNs structures mirroring their master structure (Fig. 2b). These fabricated MNs measured 554.2 ± 6.7 μm height and 182.1 ± 6.2 μm base width ($n=10$ needles), corresponding to an approximately 7% reduction in size compared with the master structure. The decrease in dimensions may be attributed to the water evaporation during the drying process, leading to solidification contraction of the HA matrix (18).

Mechanical Analysis of HA Dissolving MNs

Polymer MNs should have sufficient mechanical strength for penetrating the skin without mechanical failure. Mechanical characteristic of prepared dissolving MNs patches was evaluated using compression mode, which continuously recorded the compression force and displacement. We first measured the mechanical strengths of blank and EXT-loaded dissolving MNs. As shown in Fig. 3b, the force required to press metal cylinder against the needle increased with displacement over the range tested. The force-displacement curves showed no discontinuous point indicating needle failure, which is consistent with previous studies (18,35). For the blank MNs made of pure HA without loading drug, the compression force increased to 28.14 N when displacement reached to 400 μm. Encapsulation of 5 μg EXT in MNs of the same geometry decreased the force to 25.19 N, indicating that drug loading slightly weakened the needles strength.

We further studied the effect of water content in EXT-loaded MNs on mechanical strength due to the highly hygroscopic property of HA. After incubation in various RH conditions, the water contents in MNs changed relative to the incubation humidity (Fig. 3a), and thereby affected the mechanical properties of the MNs (Fig. 3b). The initial water levels of dried MNs (dried in silica gel) increased from 1.57 to 7.69% and 18.91% after storage at 23% and 75% RH, respectively. To reach a compression displacement of 400 μm, the required forces correspondingly reduced to 22.28 N and 8.84 N. We conclude, therefore, that the mechanical strength of HA MNs could be weakened as the water content increases, which might disable MNs insertion.

In Vitro Skin Insertion and *In Vivo* Transdermal Delivery of FAM-EXT-loaded MNs

In vitro MNs insertion ability was first evaluated by piercing the dye-loaded MNs into excised neonatal porcine skin, which is an ideal skin model for performing MNs insertion (18,19). With the aid of spring-operated applicator designed specifically for MNs insertion (Fig. 4), MNs patches were readily penetrated into the skin. Upon contact with the interstitial fluid, MNs tips rapidly dissolved and released the encapsulated dye and drug. Fig. 5a provides a representative photomicrograph of the porcine skin surface after MNs insertion. The 15 × 15 array of blue

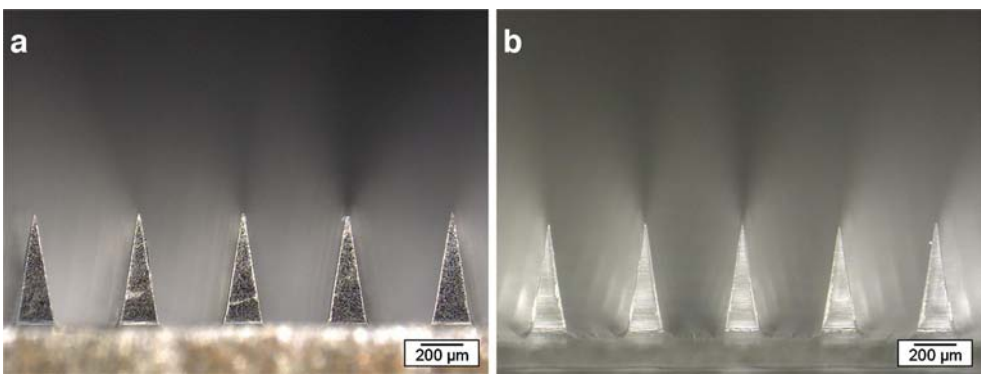

Fig. 2 Bright field micrographs of the stainless steel master structure (**a**) and the fabricated EXT-loaded dissolving MNs (**b**).

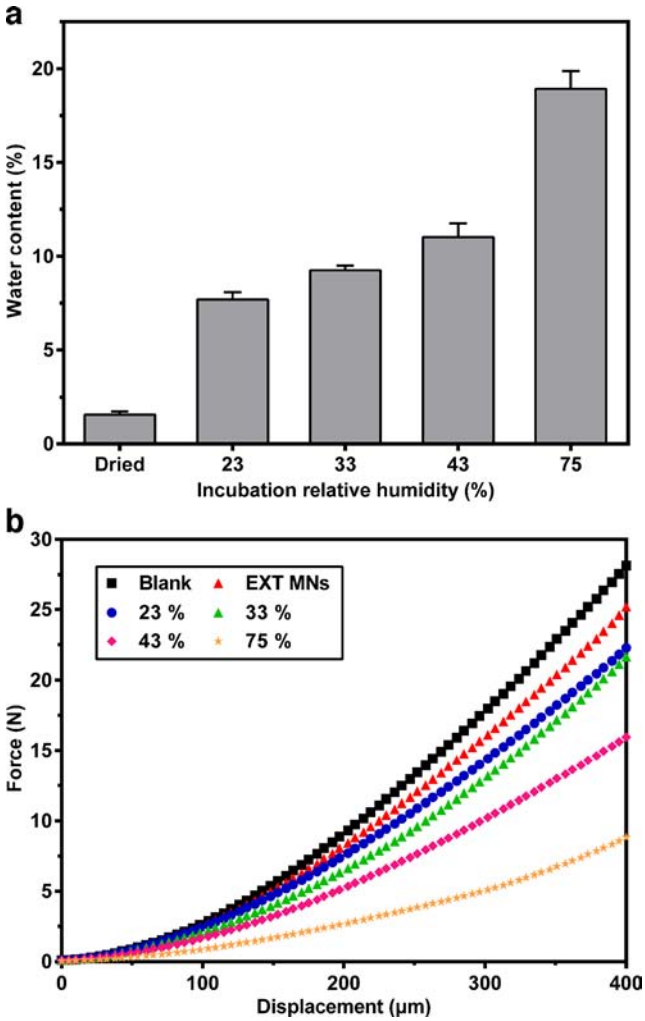

Fig. 3 Water contents and mechanical analysis of HA dissolving MNs patches. (**a**) Water contents of EXT-loaded MNs after dried in desiccators containing silica gel or incubated in various RH conditions ($n = 3$ for each group). (**b**) The force-displacement curves were measured by pressing metal cylinder probe against the MNs arrays and results represented the average of five replicate measurements each. Tested MNs included blank, EXT-loaded dissolving MNs after dried and drug-loaded MNs incubated in various RH conditions.

spots in the shape of MNs array indicates that essentially all needles were successfully inserted into the skin.

Figure 5b and c show representative fluorescence micrographs of FAM-EXT-loaded MNs before and after skin insertion for 2 min, indicating that all of the needles completely dissolved after 2 min application. To facilitate imaging the MNs insertion depth, histological sections of the skin pierced with dissolving MNs were examined. The white arrows in Fig. 5d and e show skin puncture sites by the dissolving MNs. Following dissolution, the encapsulated fluorescent dye was deposited within the skin at sites of MNs penetration and the penetration depth was approximately 280–300 μm, which means that about half of the MNs shaft penetrated into skin due to the skin deformation during MNs insertion (18).

To further assess the feasibility of *in vivo* transdermal delivery of EXT using the prepared dissolving MNs, additional experiments were performed in living rats. FAM-EXT MNs patches were inserted into the rat dorsal skin using the applicator as described above. Full-thickness skin samples were collected and then analyzed under the confocal laser scanning microscope to determine the vertical distribution of the drug in the skin. The confocal images were recorded at increasing depths from the skin surface. Fig. 5f $_{1–15}$ show the fluorescence of the released FAM-EXT and the maximal diffusion depth was at least 280 μm after insertion into rat skin for 2 min, which was consistent with Fig. 5d and e. These results indicate that the prepared HA MNs could be easily inserted into skin and then release the encapsulated drug rapidly.

In Vitro Dissolution of Drug from the EXT-loaded MNs

EXT *in vitro* dissolution from the dissolving MNs patches was performed in isolated neonatal porcine skins. The cumulative release profile was presented in Fig. 6. After insertion into the skin, the needles dissolved rapidly and released the encapsulated drug. When the insertion time extended to 2 min, almost all of the loaded EXT was released and deposited in the skin, indicating that encapsulated bioactive therapeutics could be readily delivered into the skin through the prepared HA dissolving MNs patches. Consistent with the *in vitro* dissolution result, HA dissolving MNs also completely dissolved after insertion into porcine skin for 2 min (Fig. 5c).

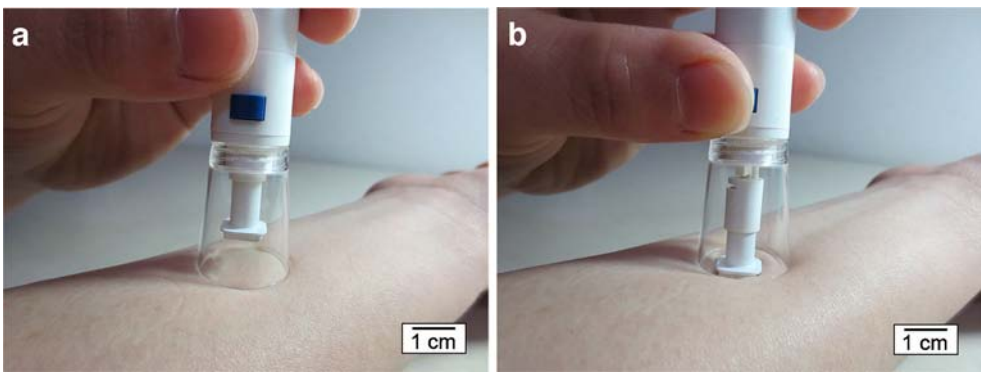

Fig. 4 Photographs of home-made spring-operated applicator used for applying dissolving MNs to skin. (**a**) The MNs patch was first attached to the applicator, and (**b**) the applicator was then activated by pressing the blue button to release the compressed spring.

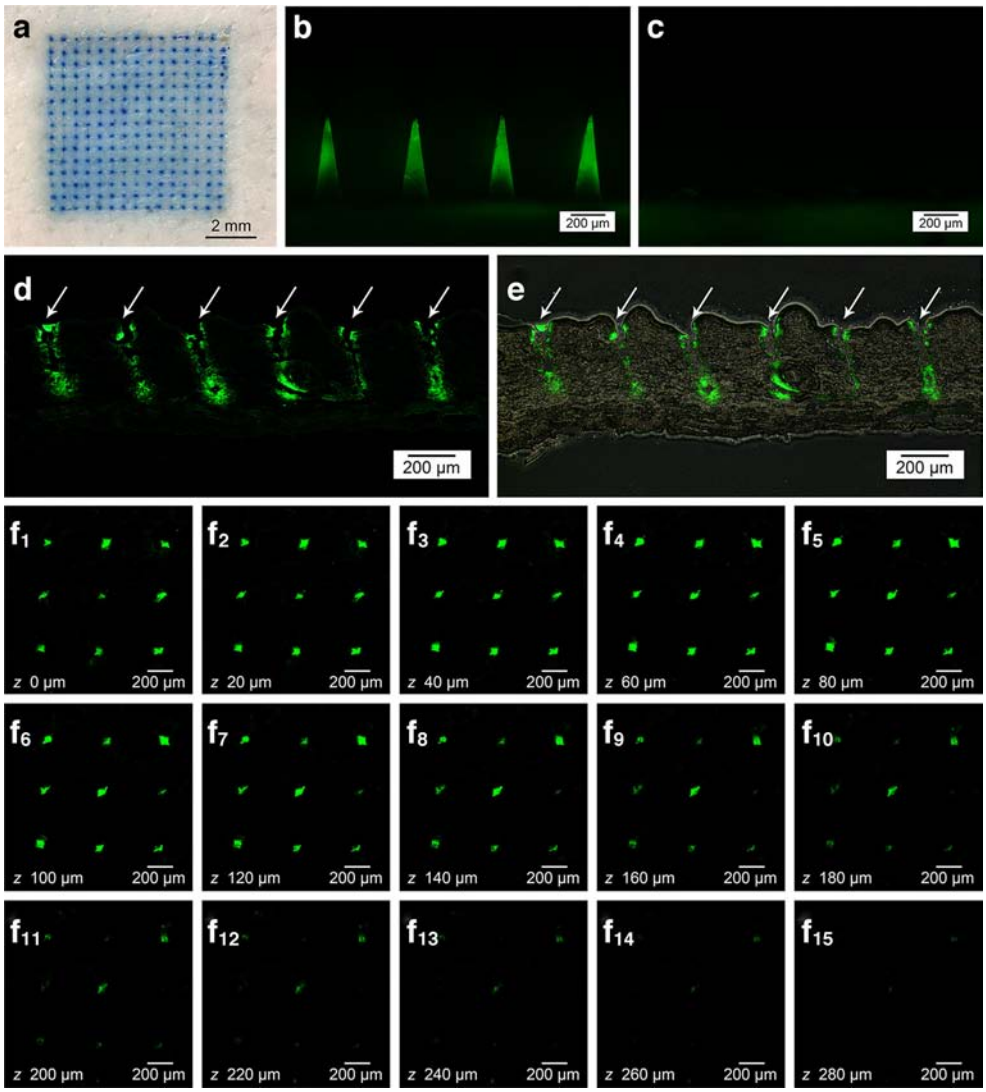

Fig. 5 *In vitro* and *in vivo* imaging of dissolving MNs insertions. (**a**) Brightfield micrograph of neonatal porcine skin after the methylene blue-loaded MNs *in vitro* insertion. Each blue spot corresponds to the site of MNs penetration into the skin. Fluorescence micrographs of FAM-EXT loaded MNs (**b**) before and (**c**) after skin insertion for 2 min. (**d**) Fluorescence and (**e**) merged brightfield and fluorescence images of histological sections of porcine skin puncture sites (white arrows). The green fluorescence in (d) and (e) indicates the FAM-EXT released from the dissolving MNs. ($\mathbf{f_{1-15}}$) Confocal laser scanning microscope images of the penetration of FAM-EXT (green) across the rat skin at different depths after *in vivo* insertion for 2 min.

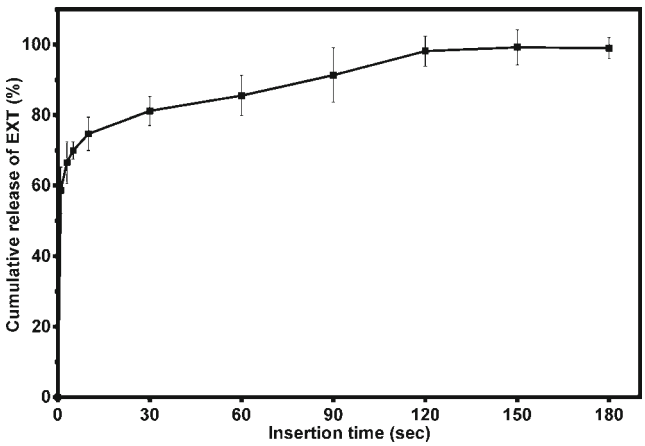

Fig. 6 *In vitro* dissolution of EXT from the rapidly dissolvable MNs in neonatal porcine skins. Each point represents the mean ± standard deviation of five replicates.

Skin Resealing Kinetics after MNs Insertions

Skin resealing kinetics after insertion of dissolving MNs in rats *in vivo* was studied using TEWL measurement. As illustrated in Fig. 7, the mean TEWL value of untreated skins was 11.02 ± 2.78 g/m^2·h before the MNs treatment. The TEWL value increased dramatically to 77.46 ± 7.68 g/m^2·h immediately after the dissolving MNs insertion. The value then gradually decreased back to a level similar to that of intact skin within 10–12 h of MNs removal, suggesting the resealing of skin's barrier properties. In contrast, the mean TEWL values of control group receiving no MNs treatment exhibited no significant change, with a minimal fluctuation around 11 g/m^2·h.

Storage Stability

For evaluation of EXT storage stability following encapsulation, drug-loaded MNs patches were stored at four different temperature conditions, with the results illustrated in Table I.

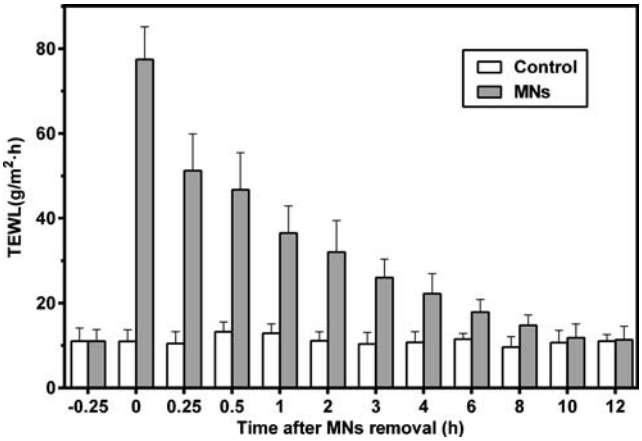

Fig. 7 Skin resealing kinetics study after insertion of EXT dissolving MNs in rats *in vivo* using TEWL measurement ($n = 6$). The TEWL values were taken at different time points pre- and post-application of MNs.

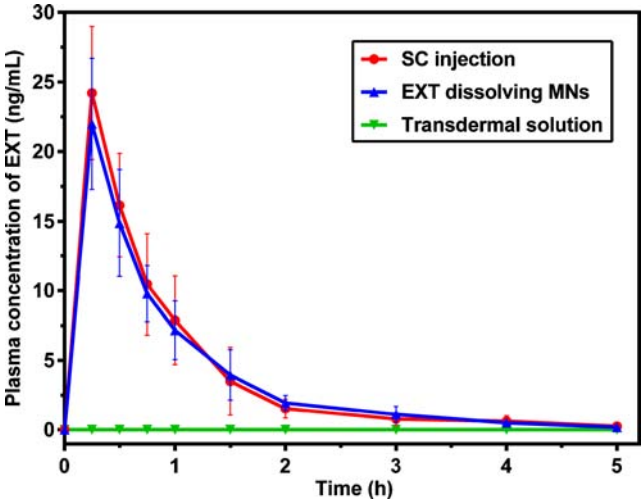

Fig. 8 The pharmacokinetic profiles of EXT in SD rats ($n = 4$ for each group) after treatment of SC injection (5 μg/20 μL), EXT-loaded MNs patches (5 μg/patch) or transdermal solution (5 μg/20 μL). Each rat received 5 μg of EXT.

The remaining percentages of the formulated EXT after 1 month of storage were 99.54, 99.79, 97.86 and 91.65% at −20, 4, 25 and 40°C, respectively. Although the remaining contents were slightly reduced at 40°C, more than 90% of encapsulated EXT remained intact in the MNs patches. Consequently, EXT encapsulated in MNs was found to be stable for at least 1 month under these storage conditions.

Transdermal Absorption of EXT in SD Rats Using Dissolving MNs Patches

To investigate transdermal absorption of EXT-loaded dissolving MNs, pharmacokinetic studies were carried out in normal SD rats. The plasma profiles and relevant pharmacokinetic parameters after administration of SC injection, EXT MNs or transdermal solution are shown in Fig. 8 and Table II. Immediately after SC injection, plasma concentrations of EXT rapidly increased, peaked at 0.25 h (C_{max} = 24.20 ± 4.79 ng/mL), and then reduced to basal level within 5 h post-injection. A similar pattern of absorption was observed after application of EXT MNs, with T_{max} and C_{max} values of 0.25 h and 22.18 ± 4.33 ng/mL, respectively (Fig. 8). In contrast, transdermal solution applied to intact skin showed undetectable levels of EXT, indicating that the drug could not be absorbed through intact rat skin. Based on calculated AUC values and initial doses, the RBA of EXT-loaded MNs was 97.06% (Table II).

Table I Storage Stability of EXT Encapsulated in Dissolving MNs Patches at Various Temperatures for 1 Month ($n = 6$)

Temperature (°C)	Remaining of EXT (%)
−20	99.54 ± 3.97
4	99.79 ± 5.87
25	97.86 ± 4.44
40	91.65 ± 1.82

Transdermal Antidiabetic Efficacy of Dissolving MNs Patches *In Vivo*

The transdermal antidiabetic effects of EXT using dissolving MNs were first investigated in non-fasting diabetic mice. Non-fasting blood glucose concentrations changes after application of placebo MNs (blank MNs with non-EXT loaded), EXT-loaded MNs or SC injection of EXT solution are illustrated in Fig. 9a. The obtained blood glucose profiles showed that both SC injection of EXT solution and application of EXT MNs lowered blood glucose levels rapidly and reached a minimum plasma glucose concentrations of approximately 42.32 ± 7.90% (from 23.20 ± 1.29 mmol/L at 0 h to 9.82 ± 1.86 mmol/L at 4 h), and 43.89 ± 9.81% (from 22.60 ± 2.67 mmol/L at 0 h to 9.87 ± 2.42 mmol/L at 5 h) of their initial values, respectively. The glucose-lowering profiles were followed by a rebound toward the pretest blood glucose values from 6 h, and returned to typical hyperglycemia at 12 h after

Table II Pharmacokinetic Parameters of EXT in SD Rats After Administration of SC Injection or Dissolving MNs Patches ($n = 4$)

	SC injection	EXT MNs patches
T_{max} (h)	0.25	0.25
C_{max} (ng/mL)	24.20 ± 4.79	22.18 ± 4.33
AUC (ng·h/mL)	20.06 ± 4.31	19.47 ± 5.11
RBA (%)	100.00	97.06

T_{max}, the time to reach maximum plasma EXT concentration

C_{max}, the maximum drug concentration

AUC, the area under the plasma EXT concentration-time curve

RBA, relative bioavailability compared with subcutaneous injection

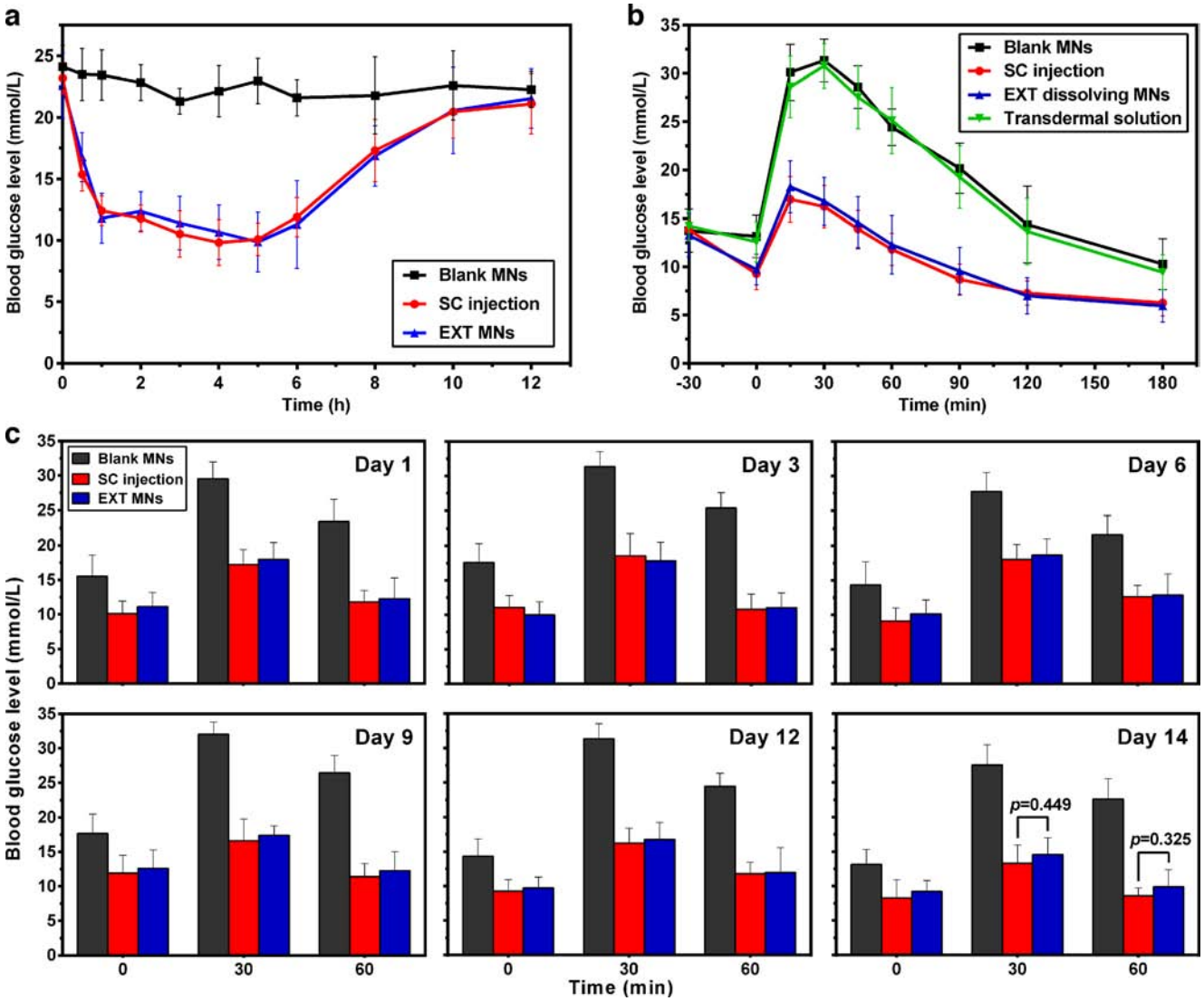

Fig. 9 Hypoglycemic effects of EXT-loaded MNs patches in *db/db* mice. (**a**) Changes in non-fasting blood glucose levels ($n = 6$ for each group) treated with blank MNs, EXT-loaded MNs patches or SC injection (5 μg EXT per mouse). (**b**) Acute glucose-lowering efficacy of different dosage regimens (5 μg EXT per mouse, $n = 5$) by OGTT. The OGTT were performed by single administering blank MNs (control), EXT-loaded MNs patches, SC injection or transdermal solution at 30 min before receiving an oral dose of glucose (1.0 g/10 mL/kg). (**c**) Long-term glucoregulatory efficacy after treated respectively with blank MNs, SC injections or EXT MNs twice everyday (10:00 am and 5:00 pm, 5 μg EXT per mouse once, $n = 5$) for 2 weeks. The OGTT were carried out after 4 h fasting from 9:00 am and blood glucose levels were monitored at 0, 30 and 60 min after glucose challenge.

administration. In contrast, the blank group (control) treated with placebo MNs showed no evident hypoglycemic action, with minimal blood glucose fluctuations (from 24.12 ± 1.75 to 21.30 ± 1.06 mmol/L).

Postprandial hyperglycemia is generally regarded as a more sensitive marker of diabetic control than the fasting glucose level in type 2 diabetes mellitus (36). The acute and long-term glucose-lowering efficacy of prepared EXT MNs patched was further investigated by OGTT in diabetic mice, with the results shown in Fig. 9b and c. For acute antidiabetic efficacy testing, an oral dose of glucose was administered to the fasted mice at 0.5 h after receiving four different dosage regimens in order to imitate the postprandial hyperglycemia, as shown in the control group received placebo MNs application. Due to no hypoglycemic activity of placebo MNs, blood glucose levels rapidly increased to 31.34 ± 2.20 mmol/L at 0.5 h after an oral glucose challenge, and then decreased slowly. However, both SC injection and EXT MNs significantly suppressed blood glucose concentrations to 16.96 ± 2.38 and 18.26 ± 2.69 mmol/L at 0.25 h after glucose challenge, respectively (Fig. 9b). Calculated glucose $AUC_{0-180\ min}$ values in Fig. 9b showed that there was no significant difference (1816.6 ± 120.0 *versus* 1872.4 ± 380.8 mmol·min/L for SC injections and EXT MNs, respectively, $p = 0.763$) between these two groups, suggesting that fabricated MNs were equally effective to conventional SC injections. In addition, the glucoregulatory effect of applying topically the EXT solution on intact skin (transdermal group) was studied as well.

Compared with the blank control, transdermal administration of EXT solution showed negligible glucose-lowering effect (3559.6±347.0 *versus* 3439.0±359.5 mmol·min/L for blank control and transdermal solution, respectively, $p=0.604$), indicating that EXT did not pass through the intact mice skin either, which is consistent with the pharmacokinetic study (Fig. 8). To investigate the long-term glucoregulatory efficacy of prepared EXT dissolving MNs, experimental *db/db* mice received twice-daily, multiple dosing of different treatments for 14 days. As in the single administration study (Fig. 9b), blood glucose concentrations of the control group treated with blank MNs markedly rose to high levels 30 min post the glucose challenges. The administrations of SC injection and EXT MNs, however, both effectively enhanced glucose tolerance, as illustrated in Fig. 9c. Furthermore, after long-term application of EXT MNs patches (Day 14 in Fig. 9c), the glucose-lowering efficacy was, as expected, almost as same as that of acute phase response (Fig. 9b or Day 1 in Fig. 9c), and there was no significant difference between the EXT MNs group and the SC injection group ($p=0.449$ for 30 min and $p=0.325$ for 60 min on Day 14). Additionally, though faint erythema was observed at application sites immediately after removal of MNs, neither damage nor irritation was identified, and these local responses disappeared 48 h after treatment (data not shown), suggesting a good tolerability profile of prepared MNs patches after long-term application *in vivo*.

DISCUSSION

Diabetes mellitus, characterized by chronic hyperglycaemia, is a complex metabolic disorder that causes increasing numbers of deaths worldwide. For patients with diabetes, hypoglycemic agents must be frequently taken to stabilize basal or postprandial glucose levels (9). EXT, as the first-in-class GLP-1 receptor agonist (incretin mimetic) approved for type 2 diabetes mellitus therapy, has multiple glucoregulatory actions, including stimulation of glucose-dependent insulin secretion, reduction of glucagon secretion, suppression of food intake and deceleration of gastric emptying. These glucoregulatory actions of EXT lower the incidence of hypoglycemia compared with traditional glucose-independent drugs such as sulfonylureas and insulin (4,37). However, the commercial product Byetta® must be SC injected twice a day due to its short half-life of 2.4 h, which adversely affects patient compliance and limits its therapeutic utility (5). To address this issue, numerous approaches have been studied to improve the therapeutic efficacy of EXT. Sustained-release dosage forms (microsphere, nanoparticles or thermogel) and structure modifications (conjugation or PEGylation to prolong the elimination half-life) of EXT are two major strategies that have been developed to reduce the administration frequency to some extent (5,34,38). Nevertheless, all of these preparations have to be administered exclusively by injection, which may still impose barriers to acceptance of therapy (6). On the other hand, attempts to delivery EXT via non-injected routes, such as oral and pulmonary routes, have also been made to enhance patient convenience and compliance (6–10). However, as mentioned previously, the bioavailabilities of EXT using these routes are limited, and the pulmonary inhalation may induce additional side effects to the lung, just like the inhaled insulin product Exubera® (24).

Transdermal delivery of biomolecules, including proteins, nucleic acids and vaccines, using dissolving MNs presents a promising alternative route, because they combine the efficacy of conventional injection with the convenience and safety of transdermal patches, while minimizing the drawbacks of both methods (16,22,32). Previous studies have reported that a variety of macromolecules, of which insulin is a representative drug, administrated by dissolving MNs, could be completely or almost completely absorbed through the skin into the systemic circulation, thus achieving a high bioavailability comparable to SC injection (24,25,32). This study, therefore, evaluated the feasibility of transdermal EXT delivery using dissolving MNs patches.

HA has been previously used as matrix material by Hiraishi *et al.* and Liu *et al.* to fabricated dissolving MNs patches (13,25–27). They demonstrated that transdermal insulin delivery and transcutaneous vaccination using the HA dissolving MNs induced comparable efficacy to traditional hypodermic injection. The safety was also verified by clinical study in healthy volunteers (27). These findings indicate that HA is suitable candidate for dissolving MNs material. It, however, took 60–120 min for their needles to completely dissolve in the skin, thus prolonging patch wearing time. As also pointed out by the authors, patients would benefit from shorter application time (13). Therefore, to increase MNs dissolution rate, we selected a different, ultralow-molecular-weight HA (5.1 kDa) produced from common HA by enzymatic degradation as the matrix material. This ultralow molecular weight HA makes it possible to minimize water content and obtain highly concentrated aqueous solutions (as high as 50–60 wt%) due to its large solubility. The high concentration solutions not only speed up the drying process, but also make the obtained MNs rapidly dissolve to release encapsulated drug within 2 min (Figs. 5c and 6), which is significantly faster than other developed dissolving MNs. This rapidly-dissolvable property makes patients complete the self-administration within several minutes, thus greatly ameliorating their convenience and compliance.

On the other hand, high hydrophilicity of HA may negatively affect the mechanical strength of dissolving MNs when they are under high humidity environments, as reported by other authors (13,25). MNs should have sufficient strength for penetrating the skin without mechanical failure. Though the morphology of MNs did not significantly change after

incubated in different humidity conditions, the water contents in MNs increased due to moisture absorption from the wet environment, thereby softening the HA matrix and reducing the MNs strength (Fig. 3b). These findings suggested that dissolving MNs patches should be sealed into water-impermeable packages to maintain their insertion ability before application. In addition to material composition, MNs geometry also affects mechanical strength. Pyramidal MNs were chosen in our study due to their superior mechanical strength compared to conical counterparts. This attribute may have to do with their larger cross-sectional area at the same base dimension. Pyramidal MNs, unlike conical MNs, generated force-displacement curves with no discontinuity, indicating that dissolving MNs underwent a progressive compression deformation (18,35).

In the MNs insertion capability studies, a home-made spring-operated applicator was used to facilitate MNs penetration by generating a high speed impact (Fig. 4). With the aid of applicator, our fabricated MNs could be readily penetrated into the skin *in vitro*/*in vivo* (Fig. 5). Histological sections of pierced skin and confocal microscopy examination showed that insertion depths were at least 280 μm, which corresponded to penetration through the *stratum corneum* and viable epidermis and into the superficial dermis. This penetration depth was generally viewed as minimally invasive and unlikely to induce pain (15,16). In addition, the measurement of TEWL demonstrated that skin's barrier properties disrupted by dissolving MNs recovered within 10–12 h (Fig. 7), suggesting that the residual micropores in the skin created by MNs puncture rapidly resealed and the damage was reversible. Furthermore, long-term multiple application of prepared MNs patches has shown a good *in vivo* skin tolerability, indicating the high safety of the HA MNs.

A critical requirement for formulations of vulnerable biotherapeutics is to preserve their functional integrity during preparation and storage (18). We used a water-based, gentle fabrication process that encapsulated fragile drug in a biocompatible matrix. This formulation limited sensitive biomolecules in dried solid state, which may be more stable than a liquid formulation (17,39). Storage stability studies showed that EXT-loaded MNs patches were not substantially degraded after storage at four different temperatures for a month, which may help diminish the need for costly, inconvenient cold chain storage (32,39). Long-term stability, however, should be further evaluated, and incorporation of sugars such as sucrose or trehalose and packaging in dry nitrogen atmosphere may further improve their storage stability (16,21,39).

Lastly, the *in vivo* pharmacokinetics and hypoglycemic efficacy of prepared MNs patches were investigated in SD rats and diabetic mice, respectively. Consistent with the *in vitro* dissolution studies in isolated porcine skins, EXT-loaded dissolving MNs also fully dissolved within 2 min after *in vivo* insertion into rat or mouse skins (data not shown). Transdermal delivery of EXT using dissolving MNs was found to achieve a high RBA of 97% (Table II), suggesting that encapsulated EXT released from MNs was almost completely absorbed through the skin into the general circulation. Hypoglycemic experiments also demonstrated that fabricated MNs were equally effective to conventional SC injections (Fig. 9), indicating that EXT retained its full activity during the MNs fabrication and dissolution. Consequently, our EXT dissolving MNs patch is an excellent alternative to traditional injection, and this minimally invasive device might also be suitable for other biotherapeutics. On the other hand, we must admit that twice-daily treatment regimen is still inconvenience and annoying for patients. Reduction of the required administration frequency through, say, structure modifications of EXT or adjustments of MNs formulation is preferred, and this further improvement would be the main aim of our future research.

CONCLUSIONS

This study seeks to assess the feasibility of transdermal delivery of EXT using HA dissolving MNs patches for type 2 diabetes mellitus therapy. The EXT preserved its functional integrity during preparation and storage due to the mild fabrication process. By choosing low-molecular-weight HA as the matrix material, our fabricated MNs could rapidly dissolve to release encapsulated drug within 2 min, thus significantly shortening administration time. In addition, *in vivo* pharmacokinetics and hypoglycemic effects studies showed that fabricated MNs were equally effective to SC injections. Overall, though clinical safety profile needs to be further evaluated, our rapidly dissolvable MNs patches would be a credible, painless alternative to conventional SC injection, and may present a non-injected option for other biotherapeutics.

ACKNOWLEDGMENTS AND DISCLOSURES

This research was supported by the Major Projects for Drug Innovation and Development from National Science and Technology of China (2014ZX09507006-002). The authors report no conflicts of interest in this work.

REFERENCES

1. DeFronzo RA. From the triumvirate to the ominous octet: a new paradigm for the treatment of type 2 diabetes mellitus. Diabetes. 2009;58(4):773–95.
2. Association AD. Diagnosis and classification of diabetes mellitus. Diabetes Care. 2008;31(Supplement 1):S55-S60.
3. Eng J, Kleinman WA, Singh L, Singh G, Raufman JP. Isolation and characterization of exendin-4, an exendin-3 analogue, from Heloderma suspectum venom. Further evidence for an exendin

receptor on dispersed acini from guinea pig pancreas. J Biol Chem. 1992;267(11):7402–5.
4. Nielsen LL, Young AA, Parkes DG. Pharmacology of exenatide (synthetic exendin-4): a potential therapeutic for improved glycemic control of type 2 diabetes. Regul Peptides. 2004;117(2):77–88.
5. Cai Y, Wei L, Ma L, Huang X, Tao A, Liu Z, *et al.* Long-acting preparations of exenatide. Drug Des Dev Ther. 2013;7:963–70.
6. Gedulin BR, Smith PA, Jodka CM, Chen K, Bhavsar S, Nielsen LL, *et al.* Pharmacokinetics and pharmacodynamics of exenatide following alternate routes of administration. Int J Pharm. 2008;356(1–2):231–8.
7. Ahn S, Lee I-H, Lee E, Kim H, Kim Y-C, Jon S. Oral delivery of an anti-diabetic peptide drug via conjugation and complexation with low molecular weight chitosan. J Control Release. 2013;170(2):226–32.
8. Nguyen H-N, Wey S-P, Juang J-H, Sonaje K, Ho Y-C, Chuang E-Y, *et al.* The glucose-lowering potential of exendin-4 orally delivered via a pH-sensitive nanoparticle vehicle and effects on subsequent insulin secretion *in vivo*. Biomaterials. 2011;32(10):2673–82.
9. Lee J, Lee C, Kim TH, Lee ES, Shin BS, Chi S-C, *et al.* Self-assembled glycol chitosan nanogels containing palmityl-acylated exendin-4 peptide as a long-acting anti-diabetic inhalation system. J Control Release. 2012;161(3):728–34.
10. Lee C, Choi JS, Kim I, Oh KT, Lee ES, Park ES, *et al.* Long-acting inhalable chitosan-coated poly(lactic-co-glycolic acid) nanoparticles containing hydrophobically modified exendin-4 for treating type 2 diabetes. Int J Nanomed. 2013;8:2975–83.
11. Hamman J, Enslin G, Kotzé A. Oral delivery of peptide drugs. BioDrugs. 2005;19(3):165–77.
12. Prausnitz MR, Langer R. Transdermal drug delivery. Nat Biotechnol. 2008;26(11):1261–8.
13. Hiraishi Y, Nakagawa T, Quan Y-S, Kamiyama F, Hirobe S, Okada N, *et al.* Performance and characteristics evaluation of a sodium hyaluronate-based microneedle patch for a transcutaneous drug delivery system. Int J Pharm. 2013;441(1–2):570–9.
14. Arora A, Prausnitz MR, Mitragotri S. Micro-scale devices for transdermal drug delivery. Int J Pharm. 2008;364(2):227–36.
15. Gill HS, Denson DD, Burris BA, Prausnitz MR. Effect of microneedle design on pain in human volunteers. Clin J Pain. 2008;24(7):585–94.
16. Kim YC, Park JH, Prausnitz MR. Microneedles for drug and vaccine delivery. Adv Drug Deliv Rev. 2012;64(14):1547–68.
17. Van der Maaden K, Jiskoot W, Bouwstra J. Microneedle technologies for (trans) dermal drug and vaccine delivery. J Control Release. 2012;161(2):645–55.
18. Lee JW, Park JH, Prausnitz MR. Dissolving microneedles for transdermal drug delivery. Biomaterials. 2008;29(13):2113–24.
19. Migalska K, Morrow DI, Garland MJ, Thakur R, Woolfson AD, Donnelly RF. Laser-engineered dissolving microneedle arrays for transdermal macromolecular drug delivery. Pharm Res. 2011;28(8):1919–30.
20. Kolli CS, Banga AK. Characterization of solid maltose microneedles and their use for transdermal delivery. Pharm Res. 2008;25(1):104–13.
21. Martin CJ, Allender CJ, Brain KR, Morrissey A, Birchall JC. Low temperature fabrication of biodegradable sugar glass microneedles for transdermal drug delivery applications. J Control Release. 2012;158(1):93–101.
22. Lee JW, Choi SO, Felner EI, Prausnitz MR. Dissolving microneedle patch for transdermal delivery of human growth hormone. Small. 2011;7(4):531–9.
23. Sullivan SP, Koutsonanos DG, Del Pilar MM, Lee JW, Zarnitsyn V, Choi SO, *et al.* Dissolving polymer microneedle patches for influenza vaccination. Nat Med. 2010;16(8):915–20.
24. Ito Y, Hirono M, Fukushima K, Sugioka N, Takada K. Two-layered dissolving microneedles formulated with intermediate-acting insulin. Int J Pharm. 2012;436(1–2):387–93.
25. Liu S, Jin MN, Quan YS, Kamiyama F, Katsumi H, Sakane T, *et al.* The development and characteristics of novel microneedle arrays fabricated from hyaluronic acid, and their application in the transdermal delivery of insulin. J Control Release. 2012;161(3):933–41.
26. Matsuo K, Yokota Y, Zhai Y, Quan Y-S, Kamiyama F, Mukai Y, *et al.* A low-invasive and effective transcutaneous immunization system using a novel dissolving microneedle array for soluble and particulate antigens. J Control Release. 2012;161(1):10–7.
27. Hirobe S, Azukizawa H, Matsuo K, Zhai Y, Quan Y-S, Kamiyama F, *et al.* Development and clinical study of a self-dissolving microneedle patch for transcutaneous immunization device. Pharm Res. 2013;30(10):2664–74.
28. Liu S, Jin M-n, Quan Y-s, Kamiyama F, Kusamori K, Katsumi H, *et al.* Transdermal delivery of relatively high molecular weight drugs using novel self-dissolving microneedle arrays fabricated from hyaluronic acid and their characteristics and safety after application to the skin. Eur J Pharm Biopharm. 2014;86(2):267–76.
29. Fraser JRE, Laurent TC, Laurent UBG. Hyaluronan: its nature, distribution, functions and turnover. J Intern Med. 1997;242(1):27–33.
30. Cohen JL, Dayan SH, Brandt FS, Nelson DB, Axford-Gatley RA, Theisen MJ, *et al.* Systematic review of clinical trials of small- and large-gel-particle hyaluronic acid injectable fillers for aesthetic soft tissue augmentation. Dermatol Surg. 2013;39(2):205–31.
31. Greenspan L. Humidity fixed points of binary saturated aqueous solutions. J Res Nat Bur Stand. 1977;81(1):89–96.
32. Ling M-H, Chen M-C. Dissolving polymer microneedle patches for rapid and efficient transdermal delivery of insulin to diabetic rats. Acta Biomater. 2013;9(11):8952–61.
33. Kehler JR, Bowen CL, Boram SL, Evans CA. Application of DBS for quantitative assessment of the peptide Exendin-4; comparison of plasma and DBS method by UHPLC–MS/MS. Bioanalysis. 2010;2(8):1461–8.
34. Chae SY, Choi YG, Son S, Jung SY, Lee DS, Lee KC. The fatty acid conjugated exendin-4 analogs for type 2 antidiabetic therapeutics. J Control Release. 2010;144(1):10–6.
35. Chen M-C, Ling M-H, Lai K-Y, Pramudityo E. Chitosan microneedle patches for sustained transdermal delivery of macromolecules. Biomacromolecules. 2012;13(12):4022–31.
36. Avignon A, Radauceanu A, Monnier L. Nonfasting plasma glucose is a better marker of diabetic control than fasting plasma glucose in type 2 diabetes. Diabetes Care. 1997;20(12):1822–6.
37. Drucker DJ, Buse JB, Taylor K, Kendall DM, Trautmann M, Zhuang D, *et al.* Exenatide once weekly *versus* twice daily for the treatment of type 2 diabetes: a randomised, open-label, non-inferiority study. Lancet. 2008;372(9645):1240–50.
38. Yu L, Li K, Liu X, Chen C, Bao Y, Ci T, *et al. In vitro* and *in vivo* evaluation of a once-weekly formulation of an antidiabetic peptide drug exenatide in an injectable thermogel. J Pharm Sci. 2013;102(11):4140–9.
39. Gill HS, Prausnitz MR. Coated microneedles for transdermal delivery. J Control Release. 2007;117(2):227–37.